

# Materials Research Express



## PAPER

# Structure, microstructure, optical and photocatalytic properties of Mn-doped ZnO nanoparticles

### OPEN ACCESS

#### RECEIVED

7 October 2019

#### REVISED

22 November 2019

#### ACCEPTED FOR PUBLICATION

4 December 2019

#### PUBLISHED

20 January 2020

Original content from this work may be used under the terms of the [Creative Commons Attribution 3.0 licence](#).

Any further distribution of this work must maintain attribution to the author(s) and the title of the work, journal citation and DOI.



S D Senol<sup>1</sup>, B Yalcin<sup>2</sup>, E Ozugurlu<sup>3</sup>  and L Arda<sup>4</sup> 

<sup>1</sup> Bolu Abant Izzet Baysal University, Faculty of Arts & Science, Department of Chemistry, 14280 Bolu, Turkey

<sup>2</sup> Bahcesehir University, Faculty of Engineering and Natural Sciences, Department of Molecular Biology and Genetics, 34353, Besiktas, Istanbul, Turkey

<sup>3</sup> Istanbul Technical University, Department of Mathematics, 34469, Maslak, Istanbul, Turkey

<sup>4</sup> Bahcesehir University, Faculty of Engineering and Natural Sciences, Department of Mechatronics Engineering, 34353, Besiktas, Istanbul, Turkey

E-mail: [lutfi.arda@eng.bau.edu.tr](mailto:lutfi.arda@eng.bau.edu.tr)

**Keywords:** hydrothermal method, diffuse reflectance spectroscopy, refractive index, photocatalytic, Urbach energy, zinc oxide

## Abstract

In this work,  $Zn_{1-x}Mn_xO$  samples were synthesized by the hydrothermal method by varying the dopant ratio from  $x = 0.01$  to  $0.05$  with  $0.01$  increment. Structural, optical and photocatalytic properties of Mn-doped ZnO were analyzed based on their concentration dependence. Structural behavior of the nanoparticles was studied by X-ray diffraction technique and it was found that  $Zn_{1-x}Mn_xO$  samples were hexagonal Wurtzite structure with no secondary phase. The effect of Mn element in  $Zn_{1-x}Mn_xO$  composition was clarified by calculating lattice parameters, cell volumes, stress, microstrain, the locality of the atoms dislocation density, displacement of atoms and bond length. SEM images revealed random agglomeration. The band gap and Urbach energies of  $Zn_{1-x}Mn_xO$  structures were determined and discussed. Different models were used to calculate refractive index and the refractive index was found in the range of  $2.05$ – $2.72$ . Mn-doped ZnO nanoparticles exhibited lower degradation rate constants ( $k = 0.0004$ – $0.0009 \text{ min}^{-1}$ ) than that of pure ZnO ( $k = 0.0014 \text{ min}^{-1}$ ). Doping Mn increased the Urbach energy value.

## 1. Introduction

The increasing demands on energy and technological applications question new materials with different doping combinations which are critical on their physical and chemical characteristics. Zinc oxide (ZnO) a widely used material with different dopant elements still keeps the importance of varying miscellaneous properties depending on synthesizing conditions, dopant rate and elements [1–5]. With the property of wide band-gap ( $3.37 \text{ eV}$ ), semiconductor ZnO occupies a special place at detector technologies with the blue and UV spectral ranges and solid-state light sources [6] and the references therein. Among the laser material technology, ZnO is one of the conventional materials for creating laser and UV light-emitting diodes with the property of  $60 \text{ meV}$  binding energy which is higher than the existing binding energy of GaN ( $25 \text{ meV}$ ) [6]. High radiation properties, thermal and chemical resistance make ZnO a preferable material in the transparent contacts of solar cells. Besides these features, ZnO and its doped forms are used in acoustic, magnetic, electric, optic, cosmetic, and nuclear applications [7–11].

Moreover, due to fast reset time, high response, photoconductive gain, and larger effective area, ZnO-based photodetectors have an important role in commercial applications when compared to the conventional or GaN [12–14] or SiC [15] photodetector technologies. In addition, to tailor the intrinsic physical properties such as electronic properties and luminescence, relevant doping elements and their rates in ZnO are essential for application purposes [16]. With the property of special electron–shell structure, rare earth [RE] ions exhibit a better luminescence center by means of their special  $f$  electron transition at different energy levels [17–20]. It is expected that Mn-doped ZnO nanostructures can be applicable to micro- and nano-optoelectronics. It is also

well known in the literature that the physical and chemical properties of doped ZnO are heavily affected by the preparation conditions, dopant rate, and dopant elements such as Cr, Co, Fe, V, Mg and Ni [1].

The researches on ZnO were triggered by doping ZnO with transition metals (TM) [21, 22]. Over the last decade, new steps were taken on revealing the useful magnetic properties convenient for industrial applications by doping ZnO with Fe, Co, and Mn elements [23–25].

Lately, an article was published by Naccarato *et al* [1] in 2019 to investigate how chemistry influences the refraction index and band gap and rationalize why certain classes of materials would execute better. Some of the refractive index calculation models were also given in Naccarato *et al* [1], namely, Ravindra *et al* [2], Moss [3], Hervé and Vandamme [4], Reddy and Anjayenu [5], Kumar and Singh [6].

In this study,  $Zn_{1-x}Mn_xO$  nanoparticles were synthesized using the hydrothermal method by varying the dopant ratio from  $x = 0.01$  to  $0.05$  with a  $0.01$  increment. The structural, optoelectronic, and photocatalytic properties of the samples were studied and the obtained results were correlated by the literature.

## 2. Experimental details

Mn-doped zinc oxide nanoparticles powders ( $Zn_{1-x}Mn_xO$ :  $x = 0.01, 0.02, 0.03, 0.04,$  and  $0.05$ ) were synthesized by hydrothermal method at different concentrations. Zinc nitrate hydrate, manganese acetate dihydrate, and hexamethylenetetramine were used as precursor materials. Deionized water was used as a solvent. After preparing the equimolar aqueous solution of the precursor materials, they were all mixed thoroughly with a magnetic stirrer for six hours at room temperature. Those solutions were transferred into the Teflon-lined autoclave. The reaction was conducted in an electric oven at  $100\text{ }^\circ\text{C}$  for 12 h. After that, Mn-doped ZnO powders were separated from the solution by using a centrifuge. Separated powders were washed with deionized water and dried in air. The powders were calcined at  $500\text{ }^\circ\text{C}$  to obtain  $Zn_{1-x}Mn_xO$  nanoparticles.

The obtained  $Zn_{1-x}Mn_xO$  nanoparticles were characterized by the Rigaku Multiflex X-ray diffraction (XRD) instrument at room temperature, with monochromated  $CuK\alpha$  ( $1.5418\text{ \AA}$ ) in the scan range of  $2\theta$  between  $20^\circ$  and  $80^\circ$  with a scan speed  $3^\circ/\text{min}$  and a step increment of  $0.02$ . The surface morphologies of the samples were evaluated by scanning electron microscopy (SEM-EDX) Jeol-6390-LV. To detail the optical properties of the samples, double beam Shimadzu 2600 UV-Spectrometer was used with an integrating sphere in  $300\text{--}700\text{ nm}$  wavelength range.

By the Perkin Elmer Spectrum Two FTIR-ATR spectrophotometer, the Fourier transform infrared (FTIR) spectra of all samples were recorded in the range of  $4000\text{--}450\text{ cm}^{-1}$ .

The photocatalytic activity of ZnO and Mn-doped ZnO ( $Zn_{1-x}Mn_xO$ ) nanoparticles were investigated based on the degradation of the Methylene Blue (MeB) as model organic dye under ambient light. The concentration of nanoparticle dispersion and methylene blue solution was  $1.0\text{ mg ml}^{-1}$  and  $1.0 \times 10^{-5}\text{ M}$  respectively. A 50 ml MeB solution was first prepared, then the appropriate amount of ZnO or  $Zn_{1-x}Mn_xO$  nanoparticles were added. The dispersion was kept in magnetic stirring in dark for 30 min to ensure the adsorption/desorption equilibrium of methylene blue on the surface of nanoparticles. Aqueous dispersions of nanoparticles containing MeB were irradiated under visible light under continuous magnetic stirring. 1.75 ml aliquots were withdrawn at appropriate time intervals; suspended ZnO or  $Zn_{1-x}Mn_xO$  nanoparticles were precipitated by centrifugation (4000 rpm for 3 min) and the absorption spectra of MeB were recorded using a Shimadzu UV mini 1240 UV-VIS spectrophotometer at a wavelength of 664 nm with deionized water as a reference. The rate of photocatalytic degradation for methylene blue was determined by the following equation [26]:

$$\ln(A_0/A) = kt$$

where  $A_0$  is the initial absorbance of MeB solution after adsorption equilibrium,  $A$  is the absorbance at the time ( $t$ ), and  $k$  is the first order photocatalytic degradation rate constant.

## 3. Results and discussion

### 3.1. Structural characterization

The structural behavior of all samples was determined by XRD analysis in the range of  $20^\circ \leq 2\theta \leq 80^\circ$  degrees. All peak positions were indexed and the second phase was not observed in all sample XRD patterns as shown in figure 1

Using XRD analysis of  $Zn_{1-x}Mn_xO$  ( $x = 0.01, 0.02, 0.03, 0.04,$  and  $0.05$ ) samples, the concentration-dependent average nanoparticle sizes, lattice parameters, volume of the unit cell, microstrain ( $\varepsilon$ ), stress ( $\sigma$ ), dislocation density ( $\delta$ ) (the amount of defect in the sample), the locality of the atoms and their displacement ( $u$ ), and bond length  $L$  were determined and reported in table 1. The detailed calculations of  $\varepsilon, \sigma, \delta, D, u,$  and  $L$  parameters were depicted in [1].

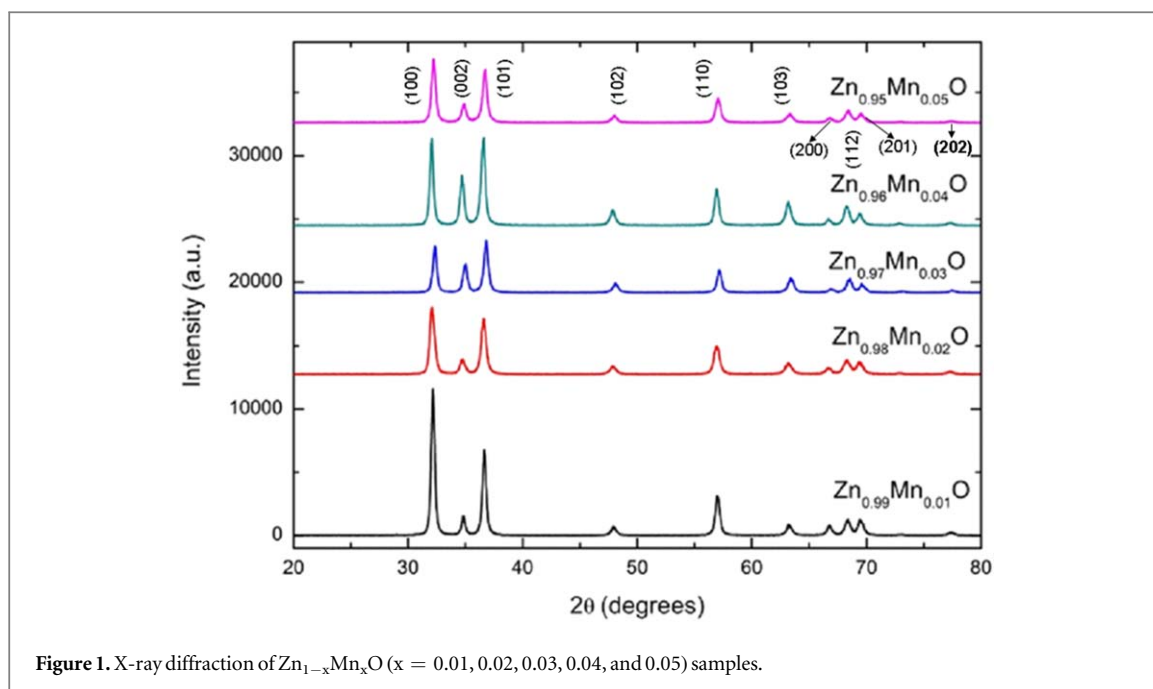


**Figure 1.** X-ray diffraction of  $Zn_{1-x}Mn_xO$  ( $x = 0.01, 0.02, 0.03, 0.04,$  and  $0.05$ ) samples.

**Table 1.** Variation in concentration-dependent average nanoparticle sizes, lattice parameters, volume of the unit cell, microstrain ( $\epsilon$ ), stress ( $\sigma$ ), dislocation density ( $\delta$ ) (the amount of defect in the sample), the locality of the atoms and their displacement ( $u$ ), and bond length  $L$  and band-gap  $E_g$  in  $Zn_{1-x}Mn_xO$  nanoparticles.

Sample name	D (nm)	a(Å)	c(Å)	c/a	R	Volume, $V(\text{Å}^3)$
$Zn_{0.99}Mn_{0.01}O$	28.36	3.24	5.19	1.602	1.019	47.1819
$Zn_{0.98}Mn_{0.02}O$	28.60	3.23	5.18	1.603	1.018	46.8007
$Zn_{0.97}Mn_{0.03}O$	28.04	3.24	5.19	1.602	1.019	47.1819
$Zn_{0.96}Mn_{0.04}O$	25.84	3.24	5.19	1.602	1.019	47.1819
$Zn_{0.95}Mn_{0.05}O$	28.86	3.24	5.20	1.605	1.017	47.2728

Sample name	$\epsilon$	$\sigma^*10^{10}(\text{N m}^{-2})$	$\delta(\text{nm}^{-2})$	$u$	$L(\text{Å})$	$E_g(\text{eV})$
$Zn_{0.99}Mn_{0.01}O$	0.0692	-1.307	$1.2433 \times 10^{-3}$	0.380	1.971	3.20
$Zn_{0.98}Mn_{0.02}O$	0.0692	-2.178	$1.2225 \times 10^{-3}$	0.380	1.966	3.19
$Zn_{0.97}Mn_{0.03}O$	0.0692	-1.307	$1.2718 \times 10^{-3}$	0.380	1.971	3.25
$Zn_{0.96}Mn_{0.04}O$	0.0747	-1.307	$1.4976 \times 10^{-3}$	0.380	1.971	3.21
$Zn_{0.95}Mn_{0.05}O$	0.0668	-4.357	$1.2006 \times 10^{-3}$	0.379	1.973	3.18

As for Mn-doped nanocrystals, the lattice parameter  $c$  was found in the range of 5.18 – 5.20 Å as shown in figure 2. There is a fluctuation in  $c/a$  lattice parameter ratio as shown in figure 3. Such fluctuations are true to be expected if Mn ions replace Zn ions in the lattice, as the Mn ions have smaller ionic radii (0.66 Å) than Zn ions (0.74 Å). The maximum microstrain  $\epsilon$  occurred at  $x = 0.04$  and before that the  $\epsilon$  values present a constant value of 0.0692 with increment Mn amount in the structure except at  $x = 0.05$ . As seen in table 1, the negative signs of  $\sigma$  values depict compressive stress and these values exhibit a decrease until  $x = 0.02$  dopant rate and after that, it is constant for  $x = 0.03$  and 0.04, it reaches the minimum value of -4.357. The fluctuations in the strain and stress values may reveal many physical defects and dislocations in the host lattice structure as shown in figure 4. Therefore, dislocation density ( $\delta$ ) describing the amount of defect in the sample was also studied. As shown in

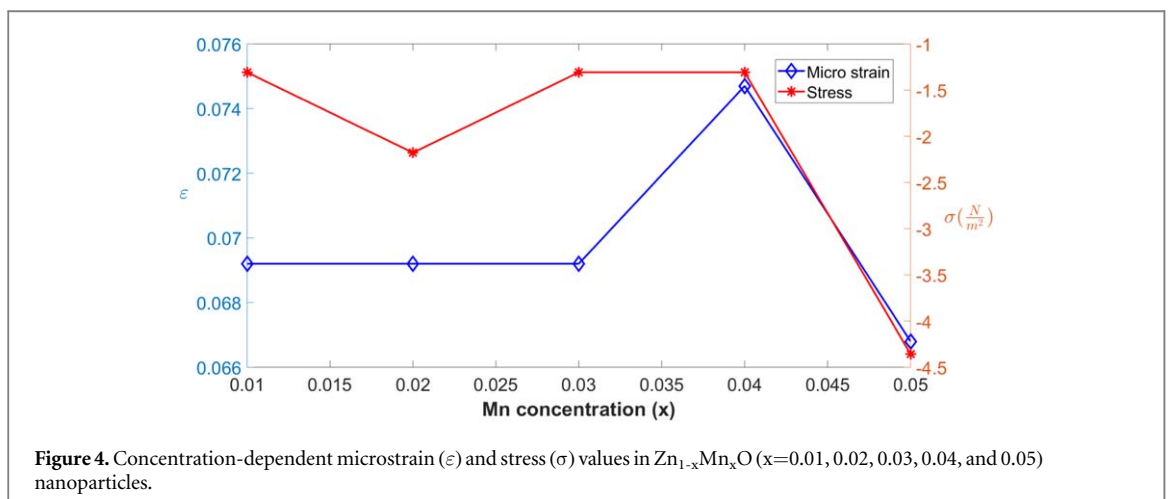
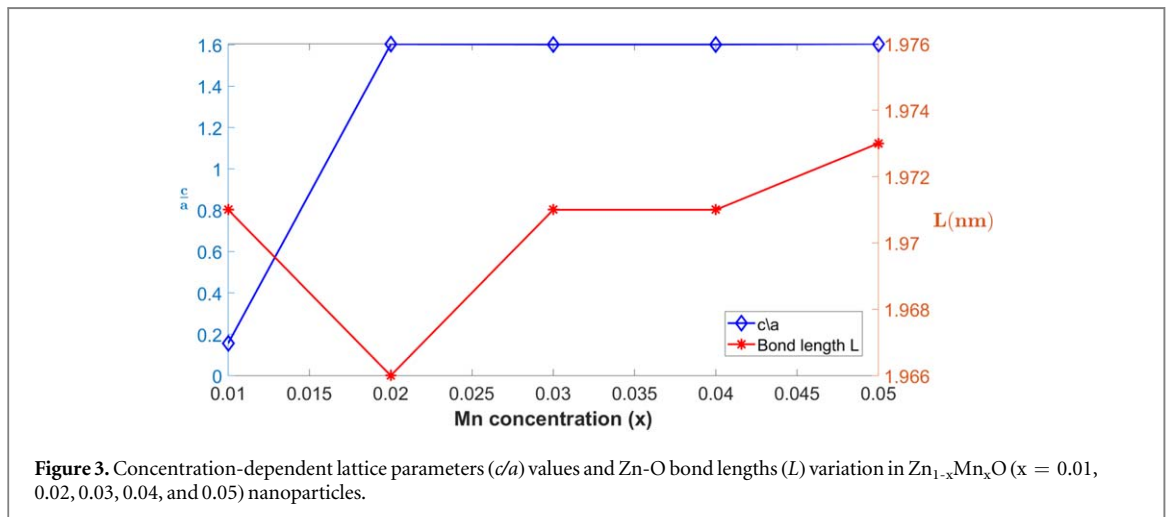
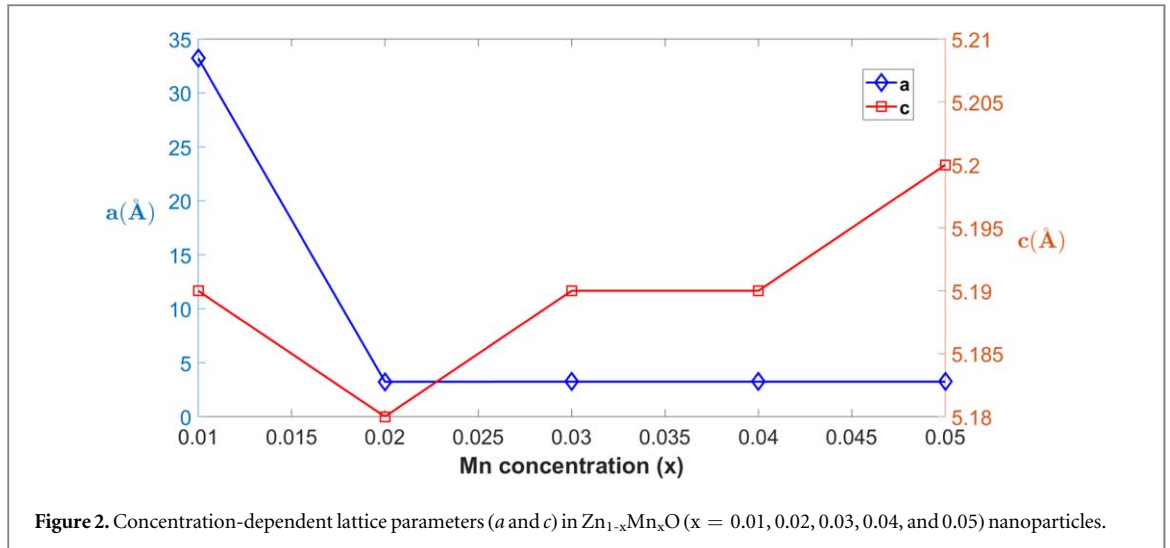


table 1, the particle's sizes ( $D$ ) of the samples are fluctuating with the increment of Mn elements in the stoichiometric samples. The maximum particle size (28.86 nm) occurs at  $x=0.05$ . At  $x=0.05$ , dislocation density ( $\delta$ ) has a minimum value of  $1.2006 \times 10^{-3}$  due to the inverse proportion expression between  $\delta$  and  $D$  values. The locality of the atoms and their displacements ( $u$  parameters) were calculated and revealed almost a constant behavior around 0.380 in  $Zn_{1-x}Mn_xO$  samples. The Zn-O bond lengths ( $L$  parameters) presented a constant value of around 1.97. The increasing dopant rate in Mn elements did not affect Zn-O bond length. The Mn-

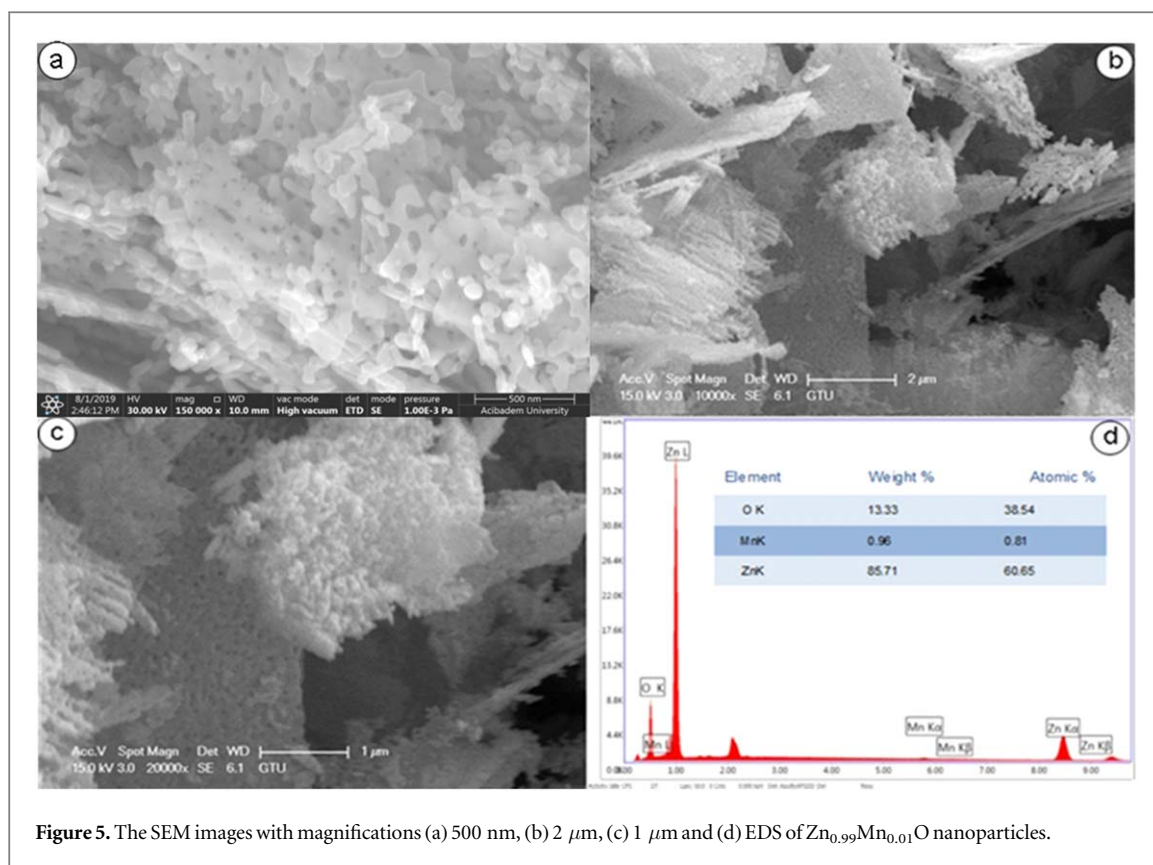


Figure 5. The SEM images with magnifications (a) 500 nm, (b) 2  $\mu\text{m}$ , (c) 1  $\mu\text{m}$  and (d) EDS of  $\text{Zn}_{0.99}\text{Mn}_{0.01}\text{O}$  nanoparticles.

doped ZnO nanoparticles have been characterized by SEM. Figures 5–9 show SEM pictures of  $\text{Zn}_{1-x}\text{Mn}_x\text{O}$  ( $x = 0.01, 0.02, 0.03, 0.04,$  and  $0.05$ ) nanoparticles. It can be seen from these figures that nanoparticles consist of holes. These nanoparticles have intertwined and tight structures. The sizes of nanoparticles are quite different from each other as well.

The composition of the  $\text{Zn}_{1-x}\text{Mn}_x\text{O}$  ( $x = 0.01, 0.02, 0.03, 0.04,$  and  $0.05$ ) nanoparticles is analyzed by EDS spectrum. EDS spectra of ZnMnO samples are depicted in figures 5(d)–9(d). Zn, Mn, and O peaks are obviously seen in the EDS spectrum. Mn peaks increase with the increasing concentration. The resulting samples have similar ratios as in the preparation of samples.

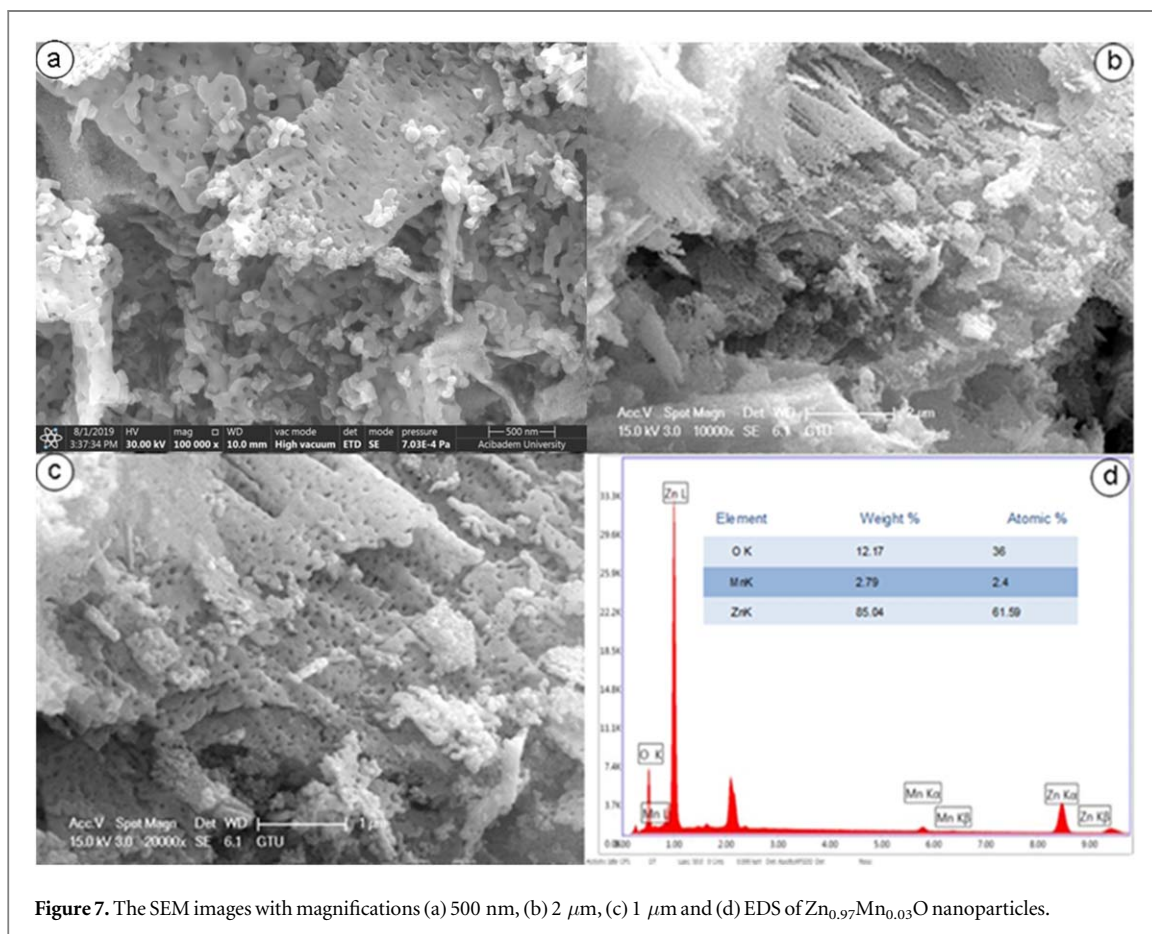
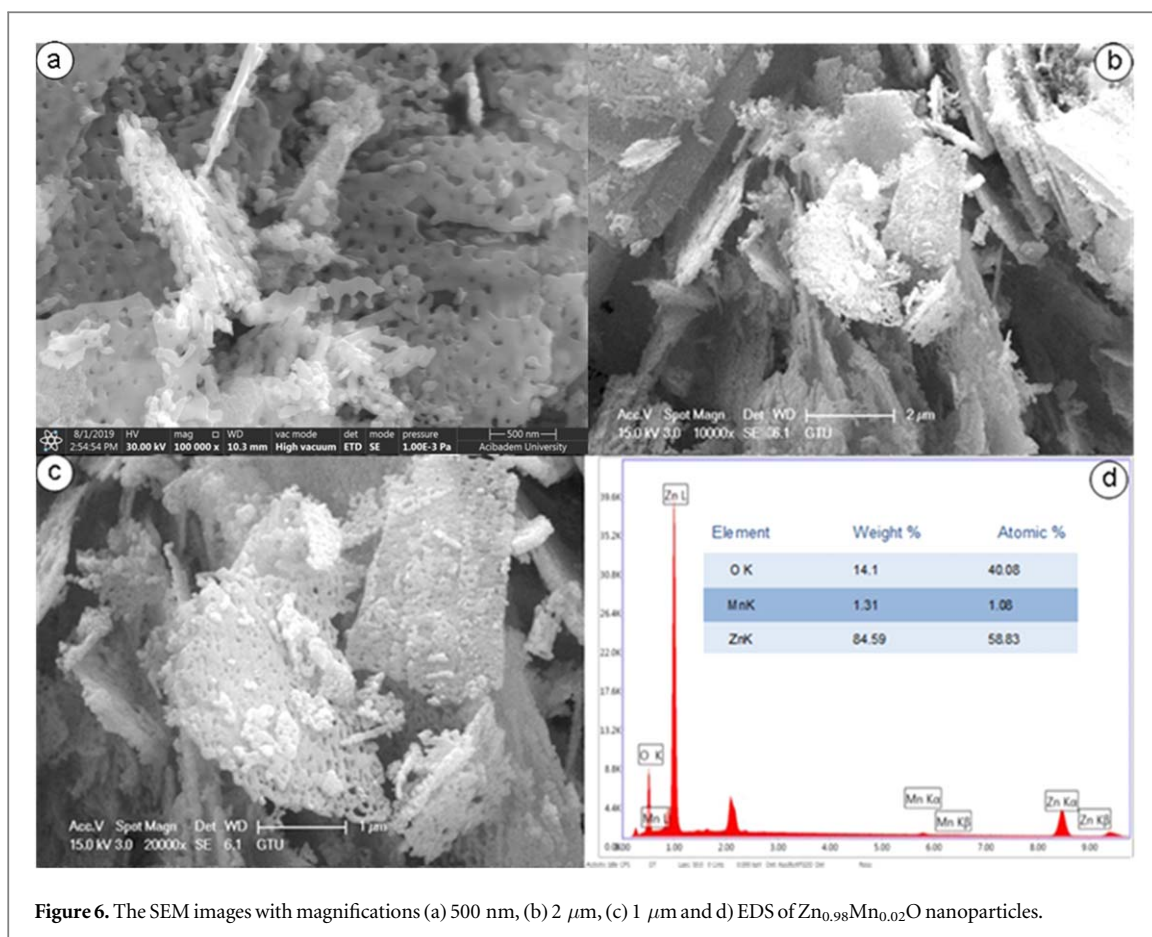
### 3.2. FTIR analysis

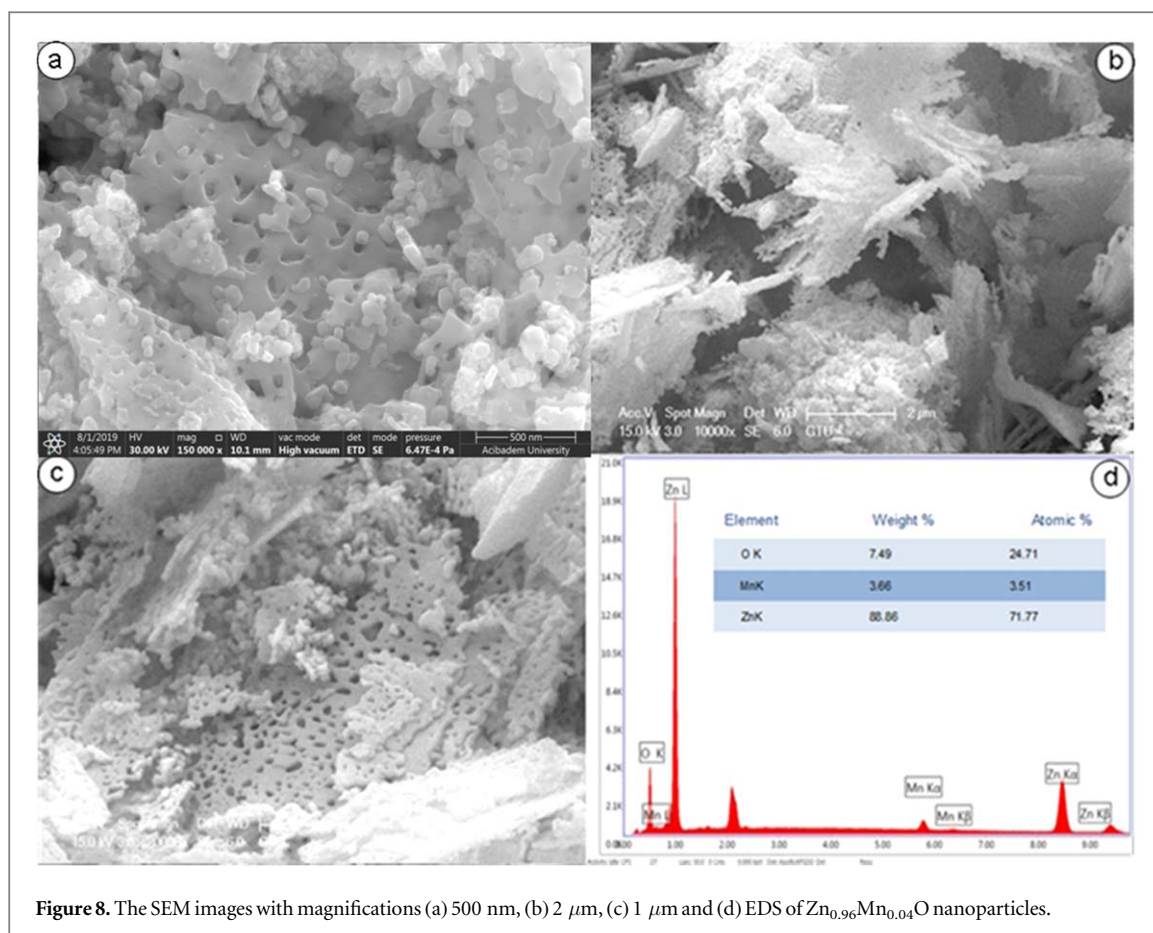
$\text{Mn}^{2+}$  doped ZnO stretching vibrations were determined by a Perkin Elmer Spectrum Two FTIR-ATR spectrophotometer at room temperature in the range of  $4000$  to  $450\text{ cm}^{-1}$  and the results are shown in figure 10.

As can be seen in detail in figure 10, the strong peak in  $450$ – $550\text{ cm}^{-1}$  range is owing to the Zn–O stretching mode, which slightly changes when  $\text{Mn}^{2+}$  is doped in the ZnO structure and the values of absorption bands are found to be  $465, 497, 504$  and  $517\text{ cm}^{-1}$ , respectively. The change in the peak position of the ZnO absorption bands exhibits that the Zn–O network is perturbed by the presence of Zn–Mn–O. Moreover, the small shift in the peak position in the doped sample may be attributed to the doping effect of metal ions. This behavior has also been reported for a study on Mn-doped ZnO [27, 28]. The small absorption peak at  $2900\text{ cm}^{-1}$  related to the  $-\text{CH}_2$  stretching modes on the surface in all samples. Another very small absorption peaks appear  $2350\text{ cm}^{-1}$  that indicates the characteristic band of  $\text{CO}_2$  molecules on the surface of the sample taken from the air atmosphere during the measurements [29]. The band located at  $850\text{ cm}^{-1}$  in all samples may be attributed to the bending vibration of nitrate (N–O); probably from the little residue of zinc nitrate used in the reaction [30].

### 3.3. Mechanism of photocatalyzation

Since methylene blue degradation predominantly occurs over the surface of photocatalytically active nanoparticles [31, 32], the organic dye-nanoparticle suspension was kept in dark in the first 30 min to avoid photodegradation. After surface adsorption/desorption equilibrium of methylene blue was achieved, the dye-nanoparticle suspension was irradiated with ambient light. Since some MeB molecules were adsorbed on the surface of nanoparticles, actual MeB concentration was considered as equal to the equilibrium concentration of this dye in the solution at the beginning of irradiation time [32].

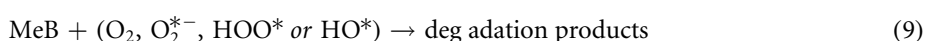
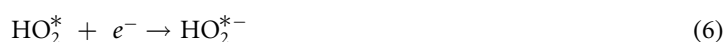
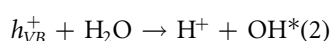


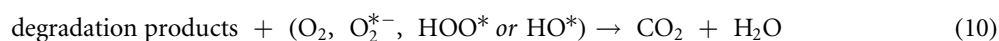
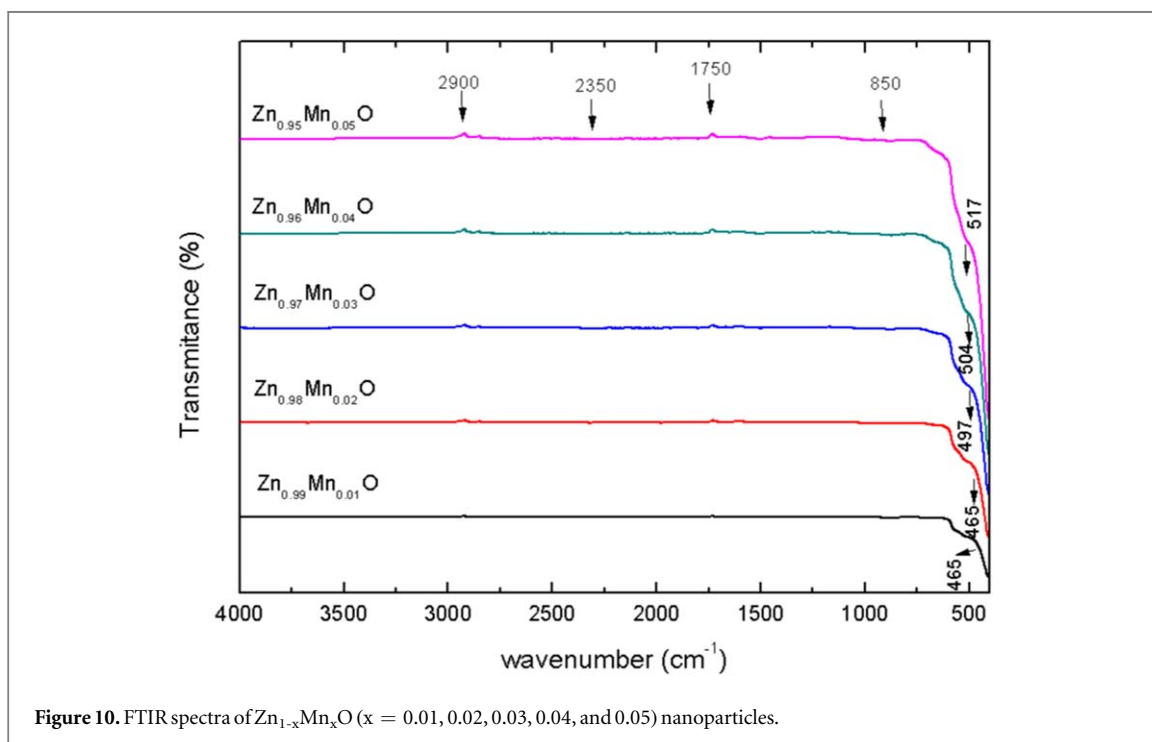
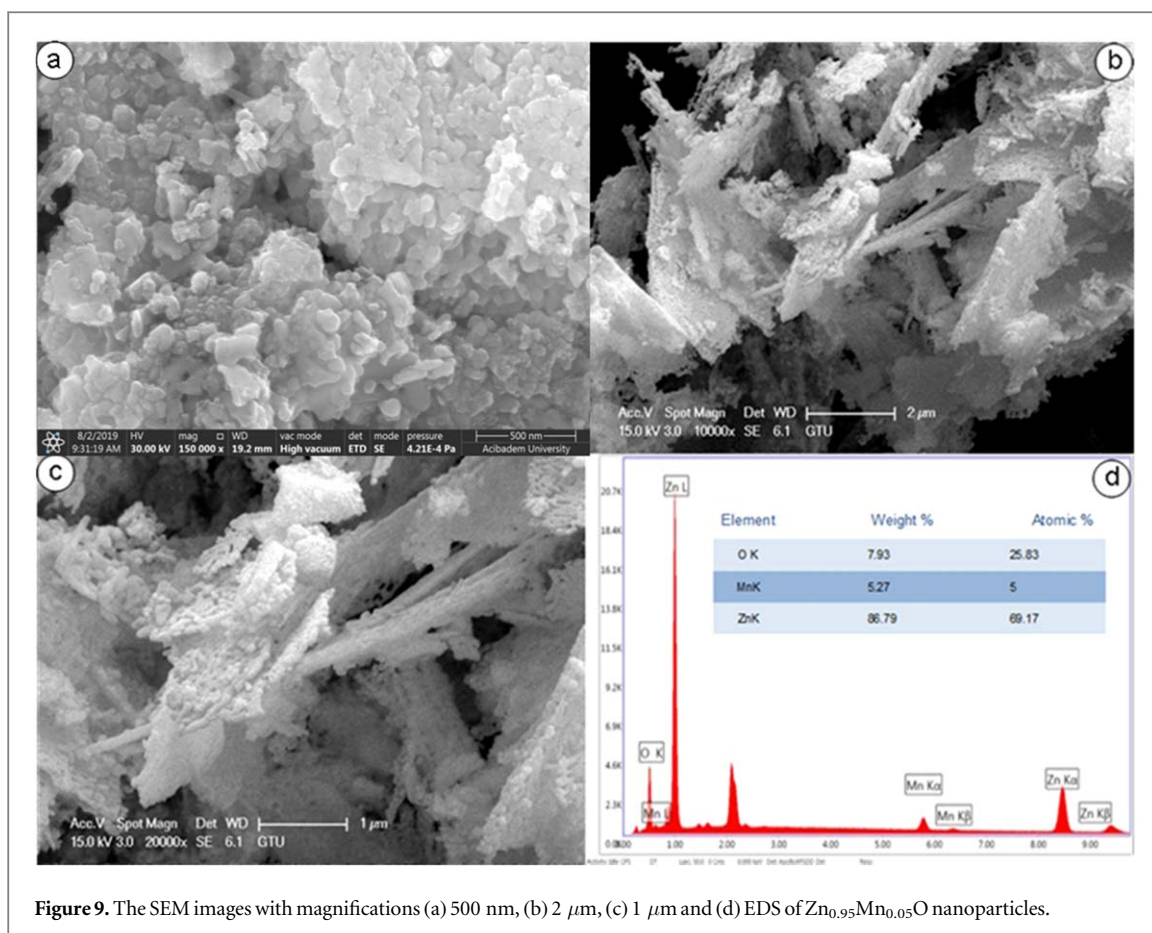


**Figure 8.** The SEM images with magnifications (a) 500 nm, (b) 2  $\mu\text{m}$ , (c) 1  $\mu\text{m}$  and (d) EDS of  $\text{Zn}_{0.96}\text{Mn}_{0.04}\text{O}$  nanoparticles.

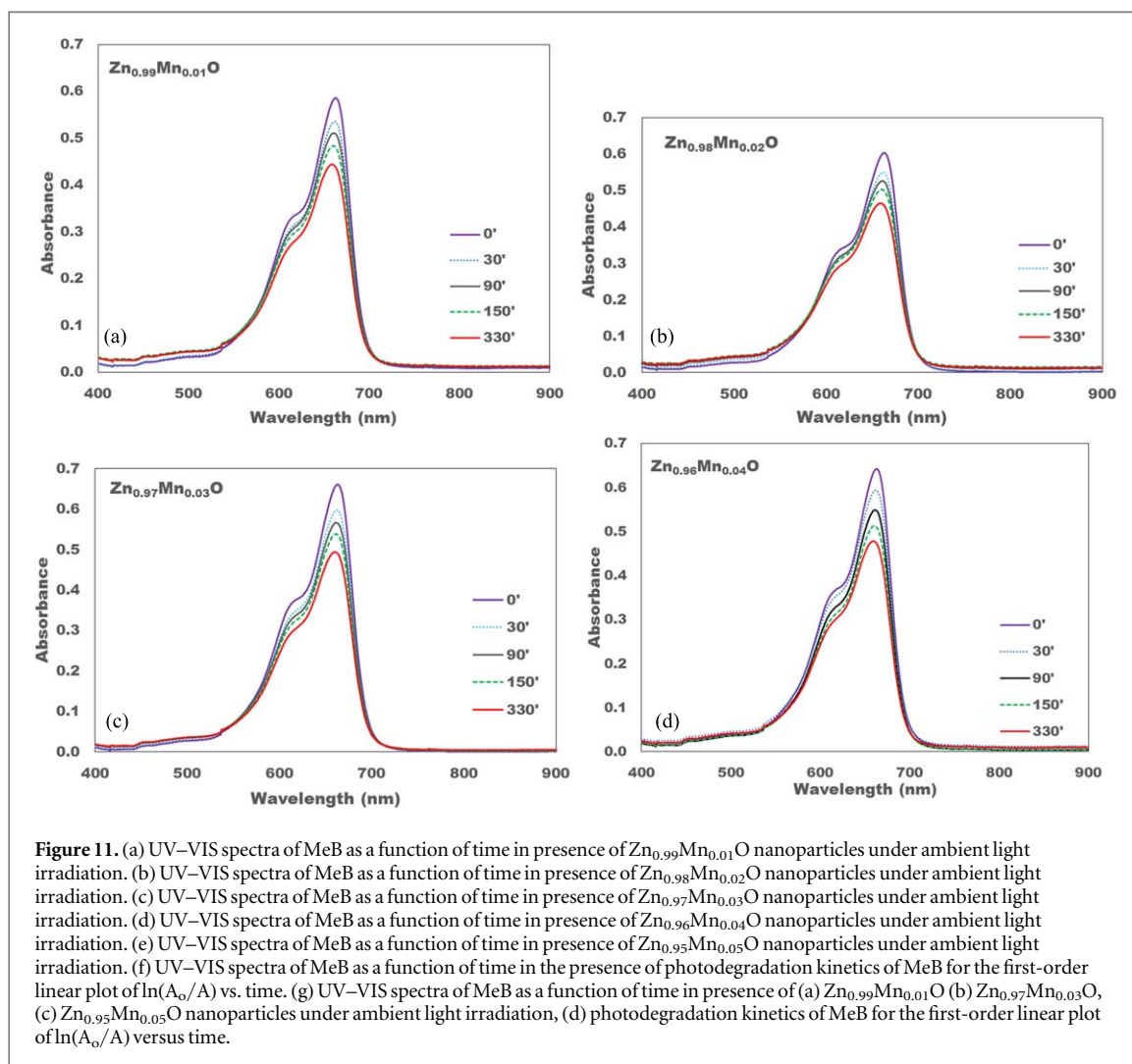
Changes in the UV-VIS spectra of non-photodegraded MeB with the variation of the time were shown in figures 11(a)–(e). Decreasing absorption band intensities corresponding to 664 nm indicated the degradation of methylene blue by both ZnO and Mn-doped ZnO nanoparticles. The intensity of the characteristic band at 664 nm significantly weakened after 330 min under the effect of ambient light irradiation by ZnO nanoparticles indicating the successful degradation of MeB.

Electron-hole pairs generated between valence bands (VB) and conduction bands (CB) of ZnO nanoparticles lead to the formation of reactive oxygen species (ROS) which are mainly responsible for the degradation of organic pollutants like MeB [33]. The first step in the formation of ROS on the surface of ZnO nanoparticles is the excitation of VB electrons with electromagnetic radiation having an energy higher than the value of the ZnO band gap ( $\sim 3.3$  eV) [34]. The migration of the excited electrons to an empty conduction band results in the formation of electron holes ( $h_{VB}^+$ ) in the VB and free electrons ( $e_{CB}^-$ ) in the CB. Electron holes and free electrons are involved in redox reactions and result in the formation of ROS like  $\text{OH}^*$ ,  $\text{HO}_2^*$ ,  $\text{O}_2^{*-}$  (equations (1)–(8)) [34–37]. These reactive oxygen species are predominantly responsible for both the degradation of organic dyes like MeB into safe degradation products like  $\text{CO}_2$  and  $\text{H}_2\text{O}$  [38] (equations (9), (10)) and antibacterial properties [39].





All  $\text{Zn}_{1-x}\text{Mn}_x\text{O}$  nanoparticles showed reduced 'visible-light-induced' photocatalytic degradation of methylene blue with degradation percentages of 13.4%–27.9% during 330 min of irradiation. The relevant degradation efficiency value for ZnO nanoparticles was 87.4%. At the same time, a linear relationship was



observed between the irradiation time and  $\ln(A_0/A)$  values indicating a pseudo-first-order kinetic [26] for the photodegradation of MeB over ZnO and  $Zn_{1-x}Mn_xO$  nanoparticles (figure 11(f)).

Table 2 shows the photocatalytic degradation rate constants for ZnO and  $Zn_{1-x}Mn_xO$  and degradation percentages of MeB in presence of these nanoparticles. Mn-doped ZnO nanoparticles exhibited lower degradation rate constants ( $k = 0.0004\text{--}0.0009\text{ min}^{-1}$ ) than that of pure ZnO ( $k = 0.0014\text{ min}^{-1}$ ) and the result was consistent with the relevant work for MeB degradation in presence of doped ZnO nanostructures [40, 41]. Reduced photocatalytic activity of  $Zn_{1-x}Mn_xO$  nanoparticles may be due to the change in the characteristics of nanoparticles caused by the  $Mn^{2+}$  doping and faster recombination of electron holes ( $h\nu_{VB}^+$ ) in the VB and free electrons ( $e_{CB}^-$ ) in the CB [42]. Another possible reason might be the generation of trapping or recombination centers for electron-hole pairs as a result of the transition metal ion substitutions in the ZnO lattice structure [43, 44].

### 3.4. Optical studies

#### 3.4.1. UV–VIS diffuse reflectance spectra

The reflectance spectra of  $Zn_{1-x}Mn_xO$  ( $x = 0.01, 0.02, 0.03, 0.04, \text{ and } 0.05$ ) nanoparticles obtained by UV–VIS diffuse reflectance measurements (DRS) in the range of 300–700 nm wavelength are shown in figure 12. Notice that all the graphs in figure 12 have an absorption edge close to 365 nm which is similar for the band gap of ZnO. Maximum reflectance was observed for  $Zn_{0.99}Mn_{0.01}O$  nanoparticles.

#### 3.4.2. Band gap calculation

The optical band gap  $E_g$  can be determined using the following equation between the absorption coefficient ( $\alpha$ ) and the photon energy ( $h\nu$ ):

$$\alpha h\nu = k(h\nu - E_g)^{1/n} \quad (11)$$

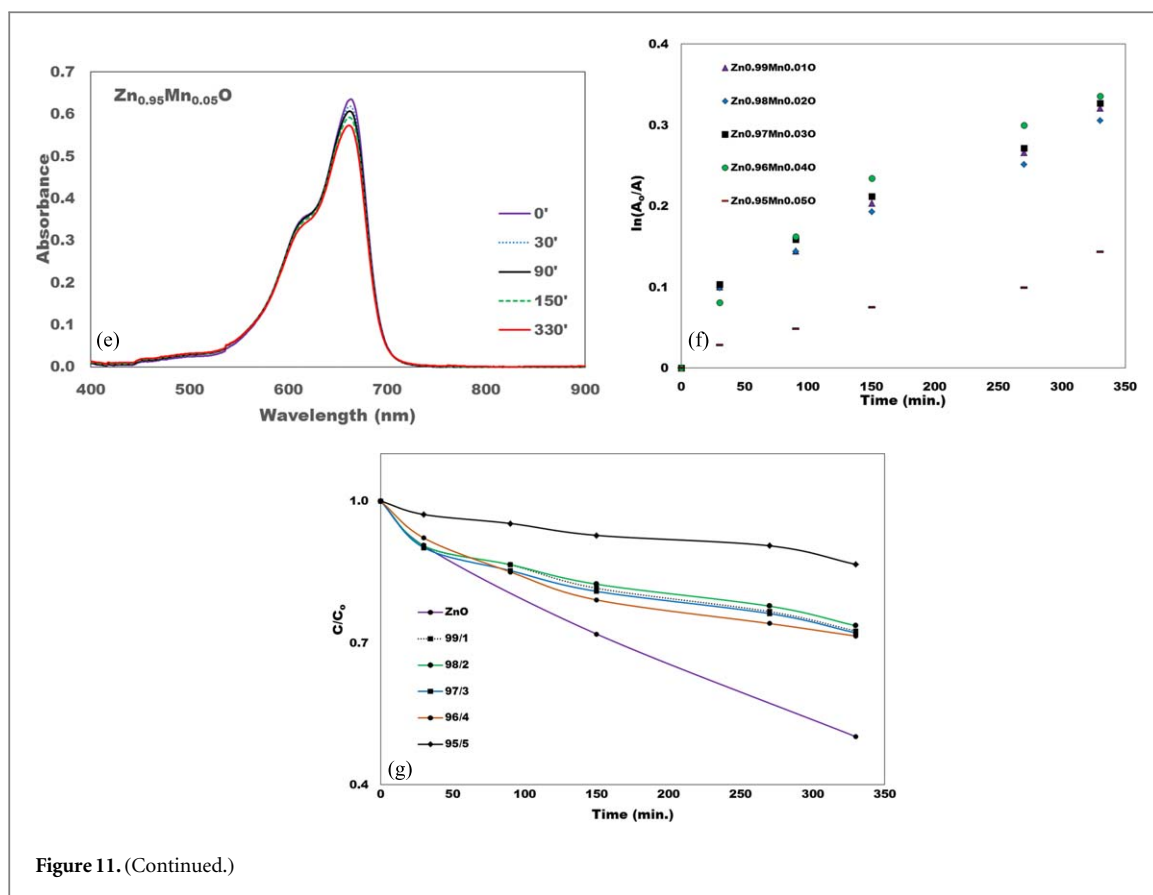


Figure 11. (Continued.)

**Table 2.** Photocatalytic degradation rate constants for ZnO and  $Zn_{1-x}Mn_xO$  and degradation percentages of MeB in presence of these nanoparticles after 330 min irradiation (photocatalyst concentration:  $0.1 \text{ mg ml}^{-1}$ ; initial concentration of MeB:  $1 \times 10^{-5} \text{ M}$ ).

	% MeB degradation	$k_{app} (\text{min}^{-1})$	$R^2$
ZnO	87.4	0.0014	0.9844
$Zn_{0.99}Mn_{0.01}O$	27.5	0.0009	0.9349
$Zn_{0.98}Mn_{0.02}O$	26.4	0.0008	0.9259
$Zn_{0.97}Mn_{0.03}O$	27.9	0.0009	0.9223
$Zn_{0.96}Mn_{0.04}O$	28.5	0.0009	0.9315
$Zn_{0.95}Mn_{0.05}O$	13.4	0.0004	0.9638

In equation (11),  $E_g$  and  $k$  are the optical band gap and energy-independent constants, respectively. Since  $F(R_\alpha)$  is proportional to  $\alpha$  and ZnO has direct allowed transitions,  $n$  is taken as  $1/2$ . Thus, equation (11) can be transformed to:

$$F(R_\alpha) h\nu = k(h\nu - E_g)^{1/2} \quad (12)$$

in other words,  $(F(R_\alpha) h\nu)^2 = k^2(h\nu - E_g)$ . The slope of the graph of  $(F(R_\alpha) h\nu)^2$  was approximated by using a linear fit  $y(h\nu) = A \times h\nu + B$  in the least-squares sense between 350 and 400 nm. To do this, the following error formula given in equation (13) was minimized for  $A$  and  $B$

$$E(A, B) = \sum_{i=1}^N [A \times (h\nu)_i + B - ((F(R_\alpha) h\nu)^2)_i]^2 \quad (13)$$

and  $A$ ,  $B$ , the variance  $\sigma^2 = \frac{E(A, B)}{N}$  values for these data set were listed in table 3 where  $N$  is the number of data points.

The band gap energies  $E_g$ , as shown in table 3 and figures 13(a)–(e), 14 and 15 are calculated by the linear approximation of the slope of the graph of  $(F(R_\alpha) h\nu)^2$  to the photon energy axis where  $F(R_\alpha) = 0$ , namely,  $E_g = h\nu = -\frac{B}{A}$ , as plotted in figures 13(a)–(e). In other words, the intersection between the linear fit and the

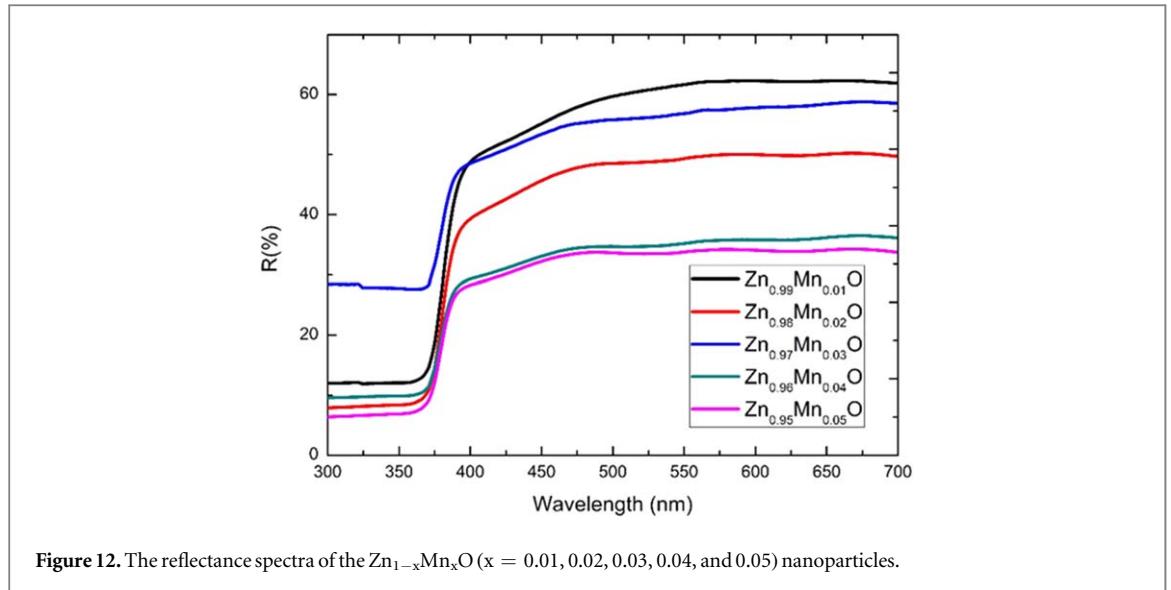


**Figure 12.** The reflectance spectra of the  $Zn_{1-x}Mn_xO$  ( $x = 0.01, 0.02, 0.03, 0.04,$  and  $0.05$ ) nanoparticles.

**Table 3.** Fitting curve function  $y(h\nu) = A \times h\nu + B$ , band gap energies, and variances for different Mn doping ratios.

Mn %	A	B	$E_g$ (eV)	$\sigma^2$
0.01	12.9147	-41.3909	3.205	$5.05 \times 10^{-4}$
0.02	6.4086	-20.4744	3.194	$1.86 \times 10^{-4}$
0.03	16.1869	-52.6264	3.251	$9.39 \times 10^{-4}$
0.04	0.2976	-0.9558	3.211	$1.91 \times 10^{-7}$
0.05	1.8616	-5.9374	3.189	$9.58 \times 10^{-6}$

photon energy axis gives the value to  $E_g$ . From figures 13(a)–(e), the band gap energies of the Mn-doped ZnO nanoparticles samples were observed to be  $3.2202 \pm 0.0309$  eV.

These changes in the values of  $E_g$  depend on several factors such as grain size, carrier concentration, lattice strain, the size effect of the dopant metals in ZnO lattice [45]. Koao *et al* [46] showed that the grain size and the luminescence intensity increased when an increase in the amount of  $Mn^{3+}$  ions occurred. Our calculations also confirmed Koao's results except at  $x = 0.05$  doping ratio in terms of the grain sizes and band gap energies.

### 3.4.3. Refractive index calculation

There has been a great interest in high refractive index  $n$  and wide band gap  $E_g$  because of their applications in optoelectronic and sensor industries. To increase the performance of optical interference filters, optical sensors (e.g. anti-reflection coatings), there is a need not only for the high refractive index but also for wide band gap materials. Lately, Naccarato *et al* [1] in 2019 published an article to relate the high refraction index and band gap, they evaluated more than 4000 semiconductors and investigated how the chemistry influences this inverse relationship between refraction index and band gap and rationalized why certain classes of materials would perform better. Naccarato *et al* [1] reviewed some of the refractive index calculation models, namely, Ravindra *et al* [2], Moss [3], Hervé and Vandamme [4], Reddy and Anjayenulu [5], Kumar and Singh [6].

Figures 16(a)–(b) exhibit the refractive index varying by Mn concentration based on these five models and the calculated values are listed in table 4. According to the findings of Naccarato *et al* [1] (See figure 5 therein), our material with ( $n > 2$  and  $E_g > 3$ ) considered in this research is classified as Transition Metals (TMs) with empty  $d$  shell (e.g.  $V^{5+}$ ).

We calculated the refraction index based on the following five models:

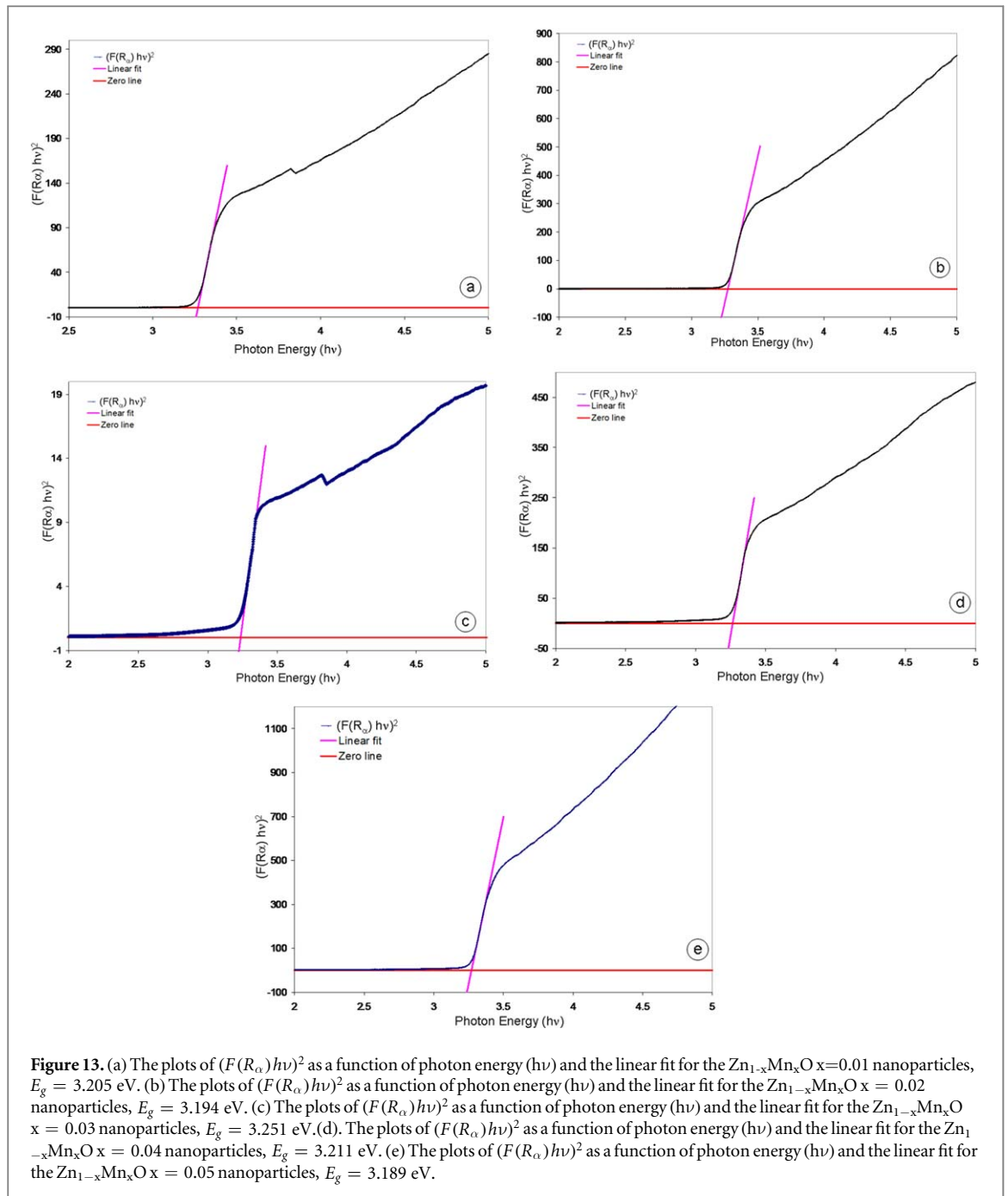
$$\text{Ravindra } et al [2] \ n = 4.084 - 0.62 E_g, \text{ Moss [3] } \ n = \left(\frac{95}{E_g}\right)^{\frac{1}{4}},$$

$$\text{Hervé and Vandamme [4] } \ n = \sqrt{1 + \left(\frac{13.6}{E_g + 3.47}\right)^2},$$

$$\text{Reddy and Anjayenulu [5] } \ n = \left(\frac{154}{E_g - 0.365}\right)^{\frac{1}{4}}, \text{ and finally}$$

$$\text{Kumar and Singh [6] } \ n = 3.3668 (E_g)^{-0.32234} \text{ and list the calculated data in table 3.}$$

Notice that the high and low refractive indices occur at Mn concentrations 0.05 and 0.03, respectively.



As shown in figures 16(a), (b), the refractive index heavily depends on the Mn concentration. The highest refractive index values were obtained at %5 Mn doping and the minimum values were obtained at %3 Mn doping.

In all figures 16(a)–(e), all five models show the same pattern between the energy band gap and refractive index. Among all these five models, Moss and Kumar and Singh give similar results in the range of 2.29–2.33. In 2015, Tripathy [47] gave the following reliability ranges for the energy band gaps based on these five models and these values were listed in table 5.

As shown in table 4, our energy band gap values are in the range of 3.20 eV and 3.26 eV, thus refractive index values based on these models are valid.

#### 3.4.4. The Urbach energy calculation

In figure 17, the logarithm of the absorption coefficient was plotted versus the photon energy eV ( $h\nu$ ) for  $Zn_{1-x}Mn_xO$  ( $x = 0.01, 0.02, 0.03, 0.04,$  and  $0.05$ ) structures. The Urbach law states that the absorption coefficient ( $\alpha$ ) near band edges is having an exponential dependence on photon energy ( $h\nu$ ), as given by the following relation:

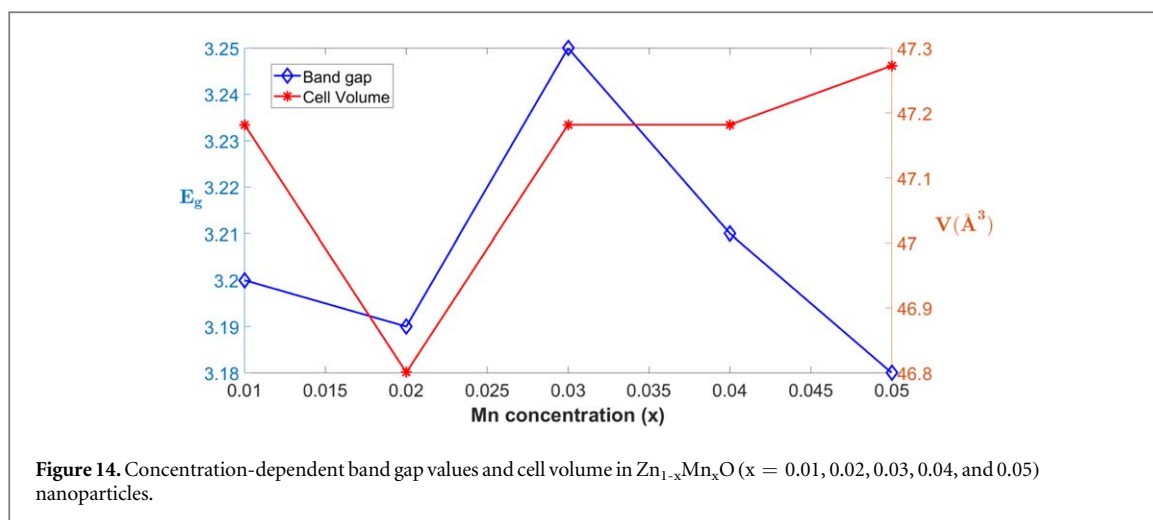


**Figure 14.** Concentration-dependent band gap values and cell volume in  $Zn_{1-x}Mn_xO$  ( $x = 0.01, 0.02, 0.03, 0.04,$  and  $0.05$ ) nanoparticles.

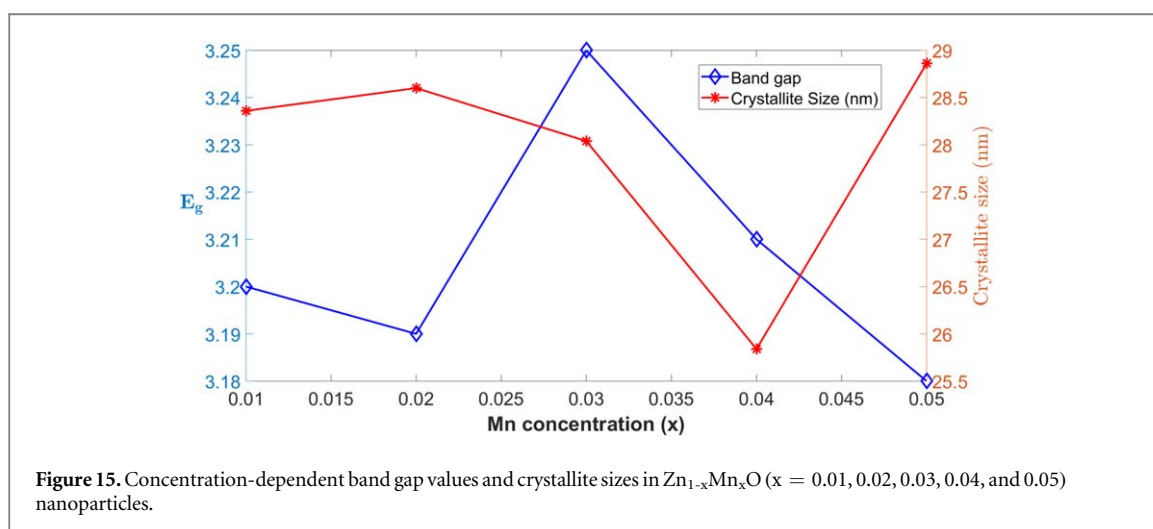


**Figure 15.** Concentration-dependent band gap values and crystallite sizes in  $Zn_{1-x}Mn_xO$  ( $x = 0.01, 0.02, 0.03, 0.04,$  and  $0.05$ ) nanoparticles.

$$\alpha = \alpha_0 e^{h\nu/E_u}$$

where  $E_u$  is the Urbach energy indicating the effect of all possible defects and  $\alpha_0$  is a constant [48]. The Urbach energy  $E_u$  values can be related to the width of the localized states in the band gap and are evaluated by using the following relation:

$$E_u = \left[ \frac{d(\ln \alpha)}{d(h\nu)} \right]^{-1}$$

where  $\alpha$  is the absorption coefficient and  $h\nu$  is the photon energy [49], and the references therein.

However, since we only know the tabulated values of the absorption coefficient, there is a need to approximate the first derivative of  $\ln \alpha$  with respect to the photon energy ( $h\nu$ ). This was done with two different finite difference methods, namely, 3-point central and 5-point formulas. The error in these approximations is of order 2 and 4, respectively. The Urbach energy values  $E_u$  were evaluated at  $E_g$  and plotted in figure 19 with band gap values as a function of Mn concentration ( $x$ ) of  $Zn_{1-x}Mn_xO$  ( $x=0.01, 0.02, 0.03, 0.04,$  and  $0.05$ ) structures, listed in table 6.

As seen in figure 18 that doping Mn increased the Urbach energy value of Mn-doped ZnO nanoparticles. The increase in  $E_u$  indicates that the structural disorder and the number of defects in the  $Zn_{1-x}Mn_xO$  structures increased with increasing concentration of Mn in the  $Zn_{1-x}Mn_xO$  structures. The highest value of Urbach energy was approximately found in the range of 774 and 839 meV for 5% Mn. Bindu and Thomas [50] found out that the value  $E_u$  was 490 meV for undoped ZnO nanoparticles. This tells us that doping Mn increases the Urbach energy value of Mn-doped ZnO nanoparticles. The increase in  $E_u$  indicates that the structural disorder and the number of defects in the  $Zn_{1-x}Mn_xO$  structures increased with increasing concentration of Mn in the  $Zn_{1-x}Mn_xO$  structures. The formation of more inter bands in between conduction and valence bands can be explained by the high value of Urbach energy.

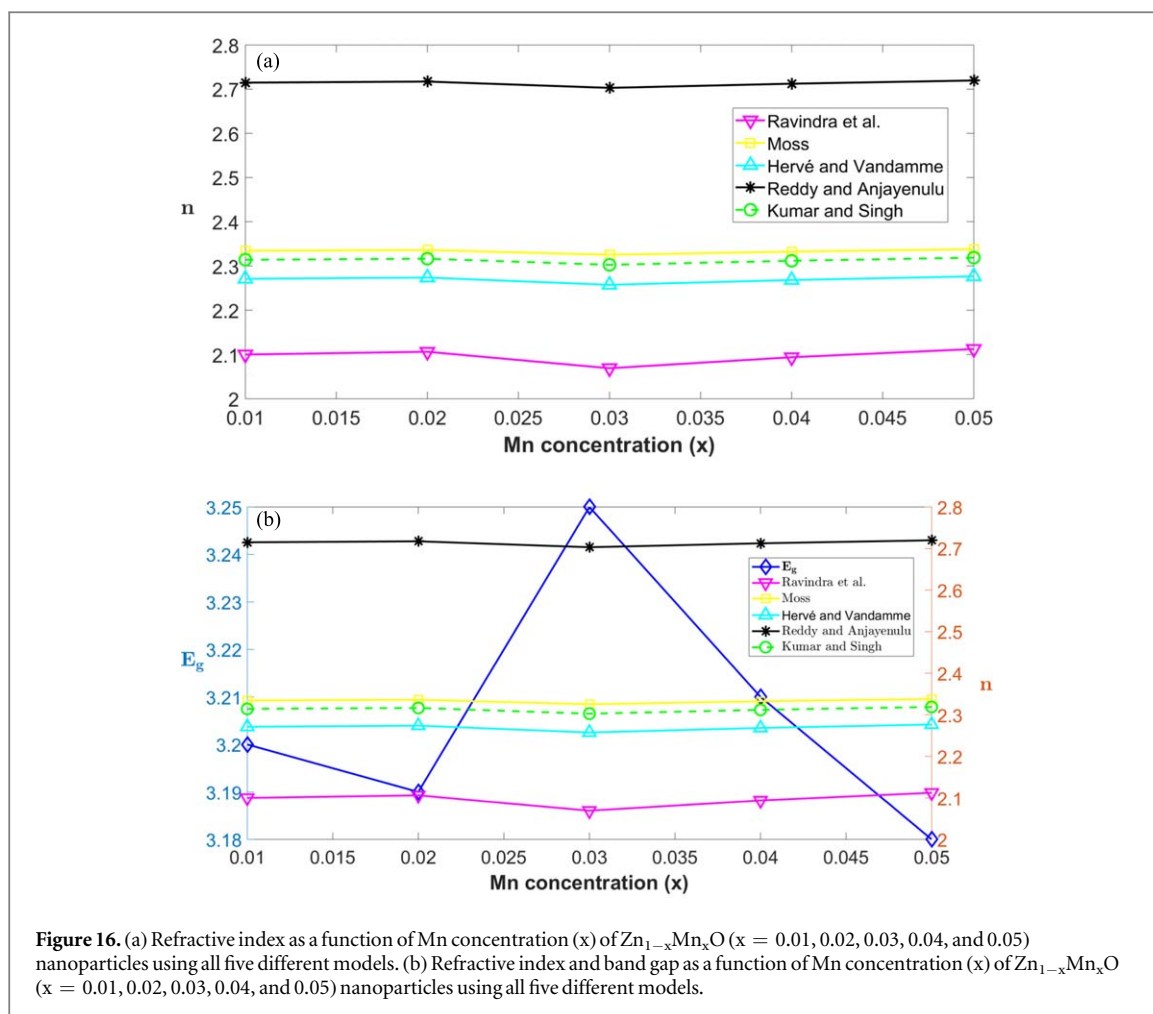


**Figure 16.** (a) Refractive index as a function of Mn concentration (x) of Zn<sub>1-x</sub>Mn<sub>x</sub>O (x = 0.01, 0.02, 0.03, 0.04, and 0.05) nanoparticles using all five different models. (b) Refractive index and band gap as a function of Mn concentration (x) of Zn<sub>1-x</sub>Mn<sub>x</sub>O (x = 0.01, 0.02, 0.03, 0.04, and 0.05) nanoparticles using all five different models.

**Table 4.** Refractive indices calculated by five different methods using band gap energies with Mn concentration.

% Mn concentration	Ravindra <i>et al</i>	Moss	Hervé and Vandamme	Reddy and Anjayenulu	Kumar and Singh	E <sub>g</sub>
1	2.1000	2.3342	2.2710	2.7148	2.3140	3.205
2	2.1062	2.3361	2.2737	2.7172	2.3164	3.194
3	2.0690	2.3252	2.2574	2.7030	2.3025	3.251
4	2.0938	2.3324	2.2683	2.7124	2.3117	3.211
5	2.1124	2.3379	2.2765	2.7196	2.3187	3.189

**Table 5.** Reliability ranges for the energy band gaps based on the models

Model	Reliability Ranges of Band Gaps
Ravindra <i>et al</i>	1.50 eV < E <sub>g</sub> < 3.50 eV
Moss	0.17 eV < E <sub>g</sub> < 3.68 eV
Hervé and Vandamme	2.00 eV < E <sub>g</sub> < 4.00 eV
Reddy and Anjayenulu	1.10 eV < E <sub>g</sub> < 6.20 eV
Kumar and Singh	2.00 eV < E <sub>g</sub> < 4.00 eV

## 4. Conclusion

Zn<sub>1-x</sub>Mn<sub>x</sub>O (x = 0.01, 0.02, 0.03, 0.04, and 0.05) nanoparticles were prepared by the hydrothermal method. Its structural, microstructural, and optoelectronic properties were analyzed based on their concentration dependence. The maximum microstrain  $\epsilon$  occurred at x = 0.04. X-ray diffraction analysis exhibited a single phase of Mn-doped ZnO nanoparticles. Moreover, the fluctuations in the strain and stress values may reveal

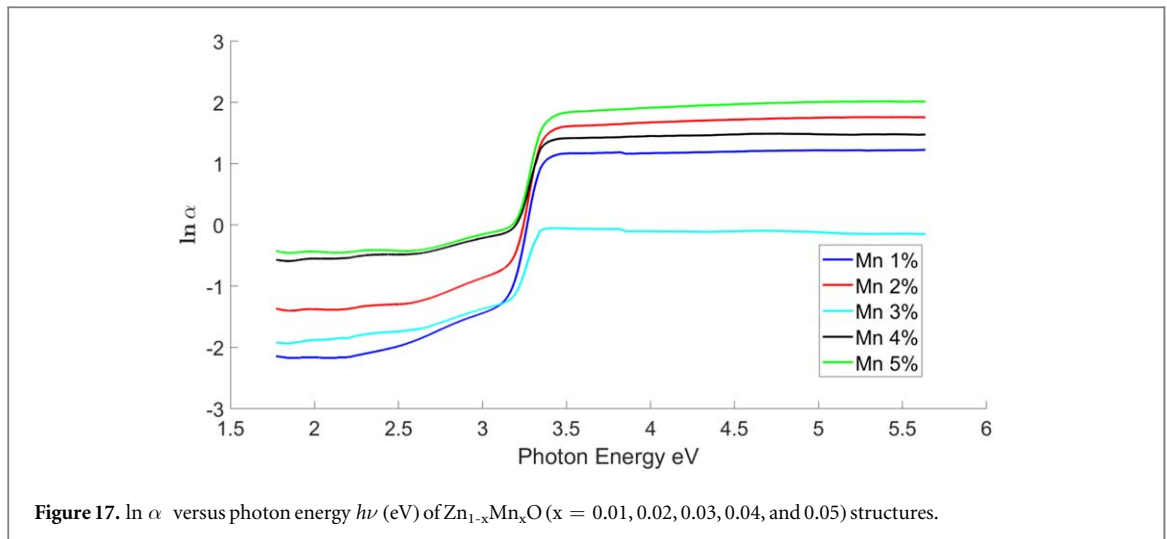


**Figure 17.**  $\ln \alpha$  versus photon energy  $h\nu$  (eV) of  $Zn_{1-x}Mn_xO$  ( $x = 0.01, 0.02, 0.03, 0.04,$  and  $0.05$ ) structures.

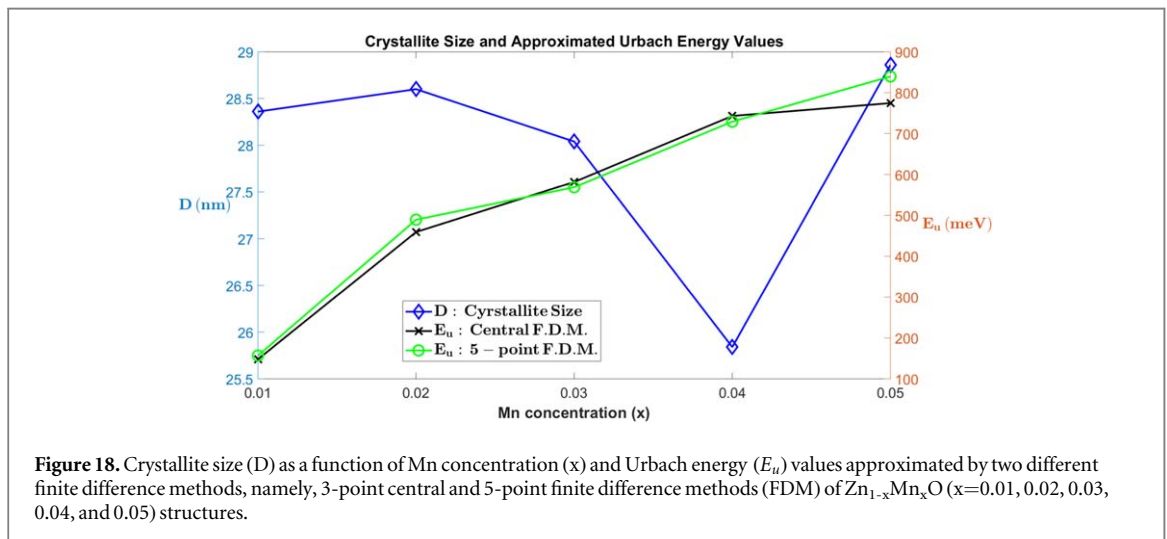


**Figure 18.** Crystallite size ( $D$ ) as a function of Mn concentration ( $x$ ) and Urbach energy ( $E_u$ ) values approximated by two different finite difference methods, namely, 3-point central and 5-point finite difference methods (FDM) of  $Zn_{1-x}Mn_xO$  ( $x=0.01, 0.02, 0.03, 0.04,$  and  $0.05$ ) structures.

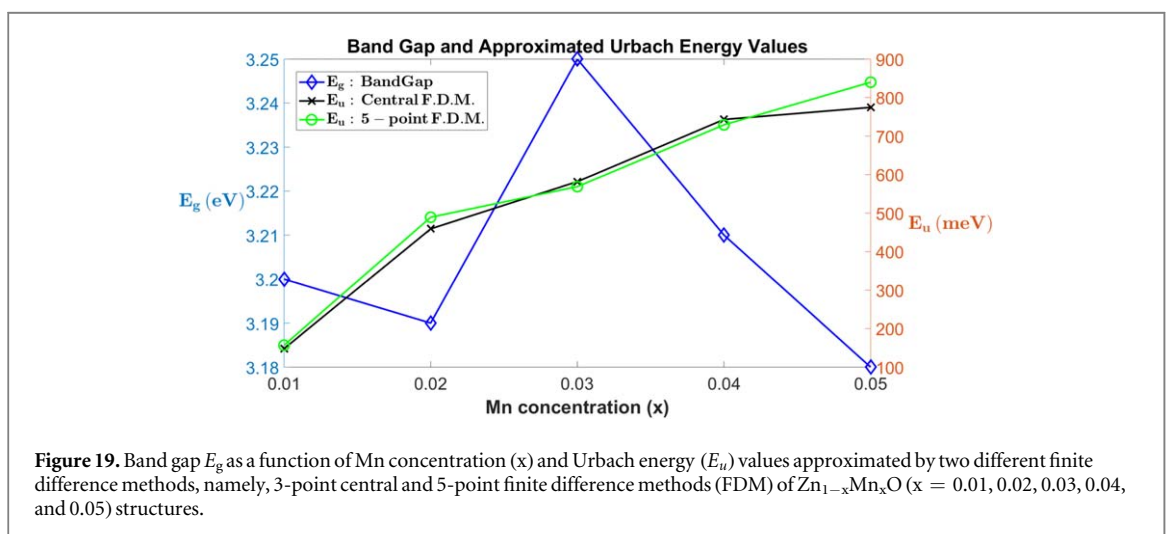


**Figure 19.** Band gap  $E_g$  as a function of Mn concentration ( $x$ ) and Urbach energy ( $E_u$ ) values approximated by two different finite difference methods, namely, 3-point central and 5-point finite difference methods (FDM) of  $Zn_{1-x}Mn_xO$  ( $x = 0.01, 0.02, 0.03, 0.04,$  and  $0.05$ ) structures.

many physical defects and dislocations in the host lattice structure. The maximum particle size (28.86 nm) occurred at  $x = 0.05$ . At  $x = 0.05$ , dislocation density ( $\delta$ ) had the minimum value of  $1.2006 \times 10^{-3}$ . The maximum band gap occurred for  $Zn_{0.97}Mn_{0.03}O$  with a band gap energy of  $E_g = 3.251$  eV. The grain sizes and the band gap energies fluctuated as the doping ratio increased. It was found that the refractive index strongly depends on the Mn concentration. At  $x = 0.01$  and  $x = 0.05$ , the maximum and minimum refractive index

**Table 6.** The Urbach energy values  $E_u$  in meV calculated at  $E_g$  by different finite difference methods (F.D.M.) for the  $Zn_{1-x}Mn_xO$  ( $x = 0.01, 0.02, 0.03, 0.04,$  and  $0.05$ ) structures.

% Mn concentration	3-point Forward F. D.M.	5-point F. D.M.
1	147.856	156.919
2	459.151	489.250
3	581.673	568.696
4	743.128	729.231
5	774.519	839.767

values were obtained, respectively. Mn-doped ZnO nanoparticles exhibited lower degradation rate constants ( $k = 0.0004\text{--}0.0009 \text{ min}^{-1}$ ) than that of pure ZnO ( $k = 0.0014 \text{ min}^{-1}$ ). The highest value of Urbach energy was approximately found in the range of 774 and 839 meV for 5% Mn.

## Acknowledgments

This research was supported by the Bolu Abant İzzet Baysal University Scientific Research Projects under the Project No: BAP- 2018.03.03.1320, and the Research Fund of Bahcesehir University (BAU-BAP.2018.02.16), Istanbul.

## ORCID iDs

E Ozugurlu  <https://orcid.org/0000-0002-1301-6963>

L Arda  <https://orcid.org/0000-0003-0722-3891>

## References

- [1] Boyraz C, Doğan N and Arda L 2017 Microstructure and magnetic behavior of (Mg/Ni) co-doped ZnO nanoparticles *Ceram. Int.* **43** 15986–91
- [2] Asikuzun E, Donmez A, Arda L, Cakiroglu O, Ozturk O, Akcan D, Tosun M, Ataoglu S and Terzioglu C 2015 Structural and mechanical properties of (Co/Mg) co-doped nano ZnO *Ceramic Inter.* **41** 6326–34
- [3] Asikuzun E, Ozturk O, Arda L and Terzioglu C 2017 Microstructural and electrical characterizations of transparent Er-doped ZnO nano-thin films prepared by sol-gel process *J. Mater. Sci., Mater. Electron.* **28** 14314–22
- [4] Heiba Z K, Arda L, Mohamed M B, Al-Jalali M A and Dogan N 2013 Structural and magnetic properties of (Al/Mg) Co-doped nano ZnO *J. Supercond Nov. Magn* **26** 3299–304
- [5] Üzar N, Algün G, Akçay N, Akcan D and Arda L 2017 Structural, optical, electrical and humidity sensing properties of (Y/Al) co-doped ZnO thin films *J. Mater. Sci., Mater. Electron.* **28** 11861–70
- [6] Rodnyi P A and Khodyuk IV 2011 Optical and luminescence properties of zinc oxide *Opt. Spectrosc.* **111** 776–85
- [7] Hassan A, Jin Y, Irfan M and Jiang Y 2018 Acceptor-modulated optical enhancements and band-gap narrowing in ZnO thin films *AIP Adv.* **8** 035212
- [8] Xiang H J, Yang J, Hou J G and Zhu Q 2006 Piezoelectricity in ZnO nanowires: a first-principles study *Appl. Phys. Lett.* **89** 223111
- [9] Nickel N H and Terukov E 2005 *Zinc Oxide—A Material For Micro- and Optoelectronic Applications* (Dordrecht: Springer)
- [10] Jeong M-C, Oh B-Y, Lee W and Myoung J-M 2005 Optoelectronic properties of three-dimensional ZnO hybrid structure *Appl. Phys. Lett.* **86** 103105
- [11] Lu H, Zhou P, Liu H, Zhang L, Yu Y, Li Y and Wang Z 2016 Effects of nitrogen and oxygen partial pressure on the structural and optical properties of ZnO: N thin films prepared by magnetron sputtering *Mater. Lett.* **165** 123–6
- [12] Ellmer E K, Klein A and Rech B 2008 *Transparent Conductive Zinc Oxide* (Berlin: Springer)
- [13] Reynolds D C, Look D C and Jogai B 2001 Fine structure on the green band in ZnO *J. Appl. Phys.* **89** 6189
- [14] Chen H, Gu S L, Tang K, Zhu S M, Zhu Z B, Ye J D, Zhang R and Zheng Y D 2011 Origins of green band emission in high-temperature annealed N-doped ZnO, *J. Lumin.* **131** 1189–92
- [15] Yun I 2012 *Photodiodes: From Fundamentals to Applications* (Rijeka: InTech)
- [16] Yim K, Lee J, Lee D, Lee M, Cho E, Lee H S, Nahm H-H and Han S Property database for single-element doping in ZnO obtained by automated first-principles calculations *Sci. Rep.* **7** 2017 40907
- [17] Blasse G 1979 *Handbook on the Physics and Chemistry of the Rare Earth* (Amsterdam: North-Holland) 4
- [18] Nazarov M I and Noh D Y 2010 Rare earth double activated phosphors for different applications *J. Rare Earths* **28** 1–11
- [19] Gogotsi Y 2006 *Nanomaterials Handbook* (USA: Routledge Publishers)
- [20] Ropp R C 1991 *Luminescence and Solid State* (USA: Elsevier Science Publishers)
- [21] Senol S D, Boyraz C, Ozugurlu E, Gungor A and Arda L 2019 Band gap engineering of Mg doped ZnO nanorods prepared by a hydrothermal method *Cryst. Res. Technol.* **1800233**
- [22] Arda L 2019 The effects of Tb doped ZnO nanorod: an EPR study *J. Magn. Magn. Mater.* **475** 493–501
- [23] Maensiri S, Laokul P and Promarak V 2006 Synthesis and optical properties of nanocrystalline ZnO powders by a simple method using zinc acetate dihydrate and poly(vinyl pyrrolidone) *J. Cryst. Growth* **289** 102–106

- [24] Senthilkumar S, Rajendran K, Banerjee S, Chini T K and Sengodan V 2008 Influence of Mn doping on the microstructure and optical property of ZnO *Mater. Sci. Semicond. Process.* **11** 6–12
- [25] Anna K, Nina P, Yuri K, Meinhard M, Werner Z and Aharon G 2008 Coating zinc oxide submicron crystals on poly(methyl methacrylate) chips and spheres via ultrasound irradiation *Ultrasound. Sonochem.* **15** 839–45
- [26] Bomila R, Suresh S and Srinivasan S 2019 Synthesis, characterization and comparative studies of dual doped ZnO nanoparticles for photocatalytic applications *J. Mater. Sci., Mater. Electron.* **30** 582–92
- [27] Ashokkumar M and Muthukumar S 2014 Microstructure, optical and FTIR studies of Ni, Cu co-doped ZnO nanoparticles by co-precipitation method *Opt. Mater.* **37** 671–8
- [28] Vijayaprasath G, Murugan R, Asaithambi S, Sakthivel P, Mahalingam T, Hayakawa Y and Ravi G 2016 Structural and magnetic behavior of Ni/Mn co-doped ZnO nanoparticles prepared by co-precipitation method *Ceram. Inter.* **42** 2836–45
- [29] Arshad M, Azam A, Ahmed A S, Mollah S and Naqvi A H 2011 Effect of Co substitution on the structural and optical properties of ZnO nanoparticles synthesized by sol-gel route *J. Alloy. Compd.* **509** 8378
- [30] Ni Y H, Wei X W, Hong J M and Ye Y 2005 Hydrothermal preparation and optical properties of ZnO nanorods *Mater. Sci. Eng. B* **121** 42
- [31] Saravanan R, Karthikeyan S, Gupta V K, Sekaran G, Narayanan V and Stephen A J M S 2013 Enhanced photocatalytic activity of ZnO/CuO nanocomposite for the degradation of textile dye on visible light illumination *Materials Science and Engineering: C* **33** 91–8
- [32] Shen W, Li Z, Wang H, Liu Y, Guo Q and Zhang Y 2008 Photocatalytic degradation for methylene blue using zinc oxide prepared by co-deposition and sol-gel methods *J. Hazard. Mater.* **152** 172–5
- [33] Nair M G, Nirmala M, Rekha K and Anukaliani A 2011 Structural, optical, photocatalytic and antibacterial activity of ZnO and Co-doped ZnO nanoparticles *Mater. Lett.* **65** 1797–800
- [34] Espitia P J P, Soares N D F F, dos Reis Coimbra J S, de Andrade N J, Cruz R S and Medeiros E A A 2012 Zinc oxide nanoparticles: synthesis, antimicrobial activity, and food packaging applications *Food Bioprocess Technol.* **5** 1447–64
- [35] Ong C B, Ng L Y and Mohammad A W 2018 A review of ZnO nanoparticles as solar photocatalysts: synthesis, mechanisms and applications *Renew. Sustain. Energy Rev.* **81** 536–51
- [36] Rajamanickam D and Shanthi M 2016 Photocatalytic degradation of an organic pollutant by zinc oxide–solar process *Arabian J. Chem.* **9** (S1) 858–68
- [37] Siwińska-Stefańska K, Kubiak A, Piasecki A, Goscińska J, Nowaczyk G, Jurka S and Jesionowski T 2018 TiO<sub>2</sub>-ZnO binary oxide systems: Comprehensive characterization and tests of photocatalytic activity *Materials* **11** 841
- [38] Saravanan R, Karthikeyan S, Gupta V K, V K, Sekaran G, Narayanan V and Stephen A J M S, 2013 Enhanced photocatalytic activity of ZnO/CuO nanocomposite for the degradation of textile dye on visible light illumination *Materials Science and Engineering: C* **33** 91–8
- [39] Padmavathy N and Vijayaraghavan R 2008 Enhanced bioactivity of ZnO nanoparticles—an antimicrobial study *Sci. Technol. Adv. Mater.* **9** 035004
- [40] Eskizeybek V, Sari F, Gülce H, Gülce A and Avcı A 2012 Preparation of the new polyaniline/ZnO nanocomposite and its photocatalytic activity for degradation of methylene blue and malachite green dyes under UV and natural sun lights irradiations *Appl. Catalysis B* **119** 197–206
- [41] Yayapao O, Thongtem T, Phuruangrat A and Thongtem S 2013 Sonochemical synthesis of Dy-doped ZnO nanostructures and their photocatalytic properties *J. Alloys Compd.* **576** 72–9
- [42] Ullah R and Dutta J 2008 Photocatalytic degradation of organic dyes with manganese-doped ZnO nanoparticles *J. Hazard. Mater.* **156** 194–200
- [43] Qiu X, Li G, Sun X, Li L and Fu X 2008 Doping effects of Co<sup>2+</sup> ions on ZnO nanorods and their photocatalytic properties *Nanotechnology* **19** 215703
- [44] Irie H, Watanabe Y and Hashimoto K 2003 Nitrogen-concentration dependence on photocatalytic activity of TiO<sub>2-x</sub>N<sub>x</sub> powders *The Journal of Physical Chemistry B* **107** 5483–6
- [45] Ziani A, Davesne C, Labbé C, Cardin J, Marie P, Portier X, Frilay C and Boudin S 2014 Annealing effects on the photoluminescence of terbium doped zinc oxide films *Thin Solid Films* **553** 52–7
- [46] Koao L F, Dejene B F, Swart H C, Motloung S V, Motaung T E and Hlangoth S P 2016 Effect Of Tb<sup>3+</sup> ions on the ZnO nanoparticles synthesized by chemical bath deposition method *Advanced Materials Letters* **77** 529–35
- [47] Tripathy S 2015 Refractive indices of semiconductors from energy gaps *Opt. Mater.* **46** 240–46
- [48] He H, Zhuge F, Ye Z, Zhu L, Wang F, Zhao B and Huang J 2006 Strain and its effect on optical properties of Al-N codoped ZnO films *J. Appl. Phys.* **99** 023503
- [49] Vettumperumal R, Kalyanaraman S, Santoshkumar B and Thangavel R 2016 Estimation of electron-phonon coupling and Urbach energy in group-I elements doped ZnO nanoparticles and thin films by sol-gel method *Mater. Res. Bull.* **77** 101–10
- [50] Bindu P and Thomas S 2017 Optical properties of ZnO nanoparticles synthesized from a polysaccharide and ZnCl<sub>2</sub> *Acta Phys. Pol. A* **131** 1474–8